

# In Vivo Versus In Vitro Degradation of a 3D Printed Resorbable Device for Ligation of Vascular Tissue in Horses

Karin H. Adolfsson, Ida Sjöberg, Odd V. Höglund, Ove Wattle, and Minna Hakkarainen\*

A resorbable 3D printed polydioxanone (PDO) device is manufactured to facilitate ligation of vascular tissue during surgery. The device must provide sufficient mechanical performance throughout the healing period. Therefore, degradation and mechanical performance of the device are investigated as a function of in vivo and in vitro aging. During aging the PDO device released cyclic and linear water-soluble products. In vivo aging resulted in higher relative number of linear oligomers in comparison to in vitro aging. A major loss of mechanical performance is observed after only 10 days in vivo and the Young's modulus (E) and tensile strength at break ( $\sigma_b$ ) decreased by 28% and 54%, respectively. This is in contrast to in vitro aging, where no loss of mechanical properties is observed during the same period. The in vivo aged devices exhibit clear holes in the matrices after 28 days, while apparent cracks are observed first after 140 days in vitro. These results highlight the sensitivity of the degradation process of resorbable devices with regards to the interactions of the device with the surrounding environment (tissues) and demonstrate the importance of in vivo testing as compliment to in vitro testing before clinical use of devices.

setting. Currently when castrating horses, the maintaining of hemostasis is often achieved by tying a resorbable thread, a suture ligature, around the vascular tissue. In this flight animal, the ligature must sustain adequate mechanical properties until the body can seal the tissue permanently. An easily applied resorbable device designed as a self-locking loop for larger vessels or vascular tissue could be a valuable surgical aid, especially when performing standing castrations in horses. Simultaneously with the reorganization of the vascular tissue, the device would ideally be hydrolyzed into low molecular weight products or metabolized,<sup>[4]</sup> which will finally lead to complete absorption of the device with a minor immunological response. A commonly used monofilament suture material is polydioxanone (PDO), a flexible, biodegradable, and biocompatible polymer.<sup>[5]</sup> A PDO suture retains sufficient tensile strength after aging both in vivo and in vitro for the first 2–3 weeks,<sup>[6–9]</sup> and is

well accepted by the tissue with a minor but transient foreign body reaction.<sup>[10,11]</sup>

In some procedures, anatomic location of a vessel makes suture ligation difficult. In such cases nonresorbable devices, i.e., polyamide cable ties have been used to facilitate ligation by tightly enclose selected vascular tissue.<sup>[12–15]</sup> However, the use of non-resorbable devices can require an additional surgical intervention to remove the device, since there are several reports on persisting foreign body reactions that may cause discomfort in the animal,<sup>[16,17]</sup> and even rejection of the implant.<sup>[18]</sup> Promisingly, it was demonstrated that a resorbable injection molded device had adequate clinical performance for ligation of blood vessels in dogs and pigs.<sup>[19–21]</sup> The advantage of a self-locking device is that it is easy to apply, hence reduces the risk of contamination and if hemostasis is not achieved on first attempt, the loop can be tightened further. This is not possible with traditional suture ligation where the tissue instead needs to be religated. However, the manufacturing process injection molding is nonflexible with respect to the possibilities to modify the design of the device.

Additive manufacturing, or 3D printing, is a technology that enables manufacturing of complex structures by a layer-by-layer approach and relatively easy modification of product design. Melt-processable thermoplastic polymers can be processed by 3D printing technique called fused filament fabrication (FFF). With respect to resorbable polymers for FFF 3D printing,

## 1. Introduction

Resorbable polymer sutures or devices are widely applied for medical purposes.<sup>[1,2]</sup> When performing surgical procedures, it is essential to maintain hemostasis, i.e., to prevent or stop major bleeding from vascular tissue or vessel. There are different types of devices used for ligating blood vessels, such as clips or electrosurgery.<sup>[3]</sup> The major drawbacks with these devices is that they are designed for smaller vessels and require a hospital

K. H. Adolfsson, M. Hakkarainen  
Department of Fibre and Polymer Technology  
KTH Royal Institute of Technology  
Stockholm 100 44, Sweden  
E-mail: minna@kth.se

I. Sjöberg, O. V. Höglund, O. Wattle  
Department of Clinical Sciences  
SLU Swedish University of Agricultural Sciences  
Uppsala, Box 7054, 750 07, Sweden

 The ORCID identification number(s) for the author(s) of this article can be found under <https://doi.org/10.1002/mabi.202100164>

© 2021 The Authors. Macromolecular Bioscience published by Wiley-VCH GmbH. This is an open access article under the terms of the Creative Commons Attribution License, which permits use, distribution and reproduction in any medium, provided the original work is properly cited.

DOI: 10.1002/mabi.202100164

polylactide (PLA) and polycaprolactone (PCL) are the most common materials.<sup>[22]</sup> The possibility to 3D print resorbable polymers has opened up a wide range of opportunities to transform digital models into unique and complex on-demand surgical devices with high flexibility to customize the design for different applications and patients, but there is still a demand for a greater diversity in 3D printable resorbable polymers. The prerequisites for a resorbable 3D printed device for the application requirements, in addition to suitable degradation rate and 3D printability, are biocompatibility and sufficient mechanical strength. It is further important to minimize thermo-mechanical batch variations.<sup>[23]</sup>

3D printing of PDO has previously been successfully demonstrated.<sup>[5]</sup> The in vitro aging under accelerated conditions showed similar degradation rates between PDO and glycoside/lactide based devices, whereas more hydrophobic polymeric devices based on caprolactone and lactide displayed slower degradation rates. In addition to common in vitro aging studies, the correlation to in vivo experiments is important.<sup>[24]</sup> Studies of the in vivo and in vitro behavior of FFF 3D printed PCL showed promising results for bone formation after introduction of  $\beta$ -tricalcium phosphate<sup>[25]</sup> and chitosan hydrogel.<sup>[26]</sup>

Manufacturing by 3D printing offers the possibility to design and customize precise resorbable surgical devices. However, the in vivo and in vitro degradation studies on FFF 3D printed resorbable polymers are scarce. Our postulation was that the type of manufacturing will affect the degradation rate and mechanical performance of the device originally and over time. Establishing these correlations are of outermost importance for the function of a surgical device for providing hemostasis, while reorganization of vascular tissues. Furthermore, outer conditions, such as surrounding environment, greatly influence the degradation of resorbable polymers. A comprehensive in vivo and in vitro study of a 3D printed PDO device for ligation of vascular tissues in horses was conducted. The degradation profile and mechanical performance of the PDO device were evaluated and compared between the different conditions. The influence of two different macroscopic morphologies on the degradation of the device were further studied.

## 2. Experimental Section

### 2.1. Materials

The 3D printed PDO device was bought from Poly-Med Inc. Sarstedt tubes of polypropylene (PP) was purchased from Kruse. Prolene PP suture was bought from Ethicon. All materials and other chemicals were used as received.

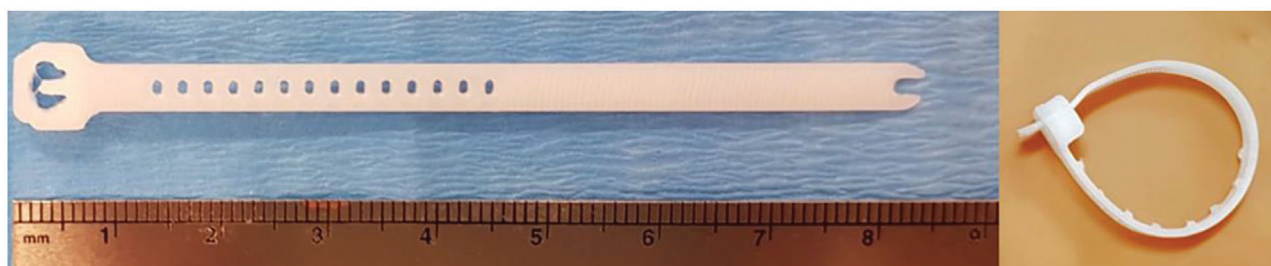


**Figure 1.** Images of the 3D printed device.

**Table 1.** 3D printing parameters of the PDO device adapted by Poly-Med.

3D printing parameters	
Printing temperature	165 °C
Fan cooling	80%
Extrusion width	0.3 mm
Nozzle size	0.25 mm
Infill percentage	100%
Infill angle	0; 90°
Infill pattern	Rectilinear
Shell/perimeter	2
Layer height	0.15 mm
First layer height	0.15 mm
Bottom solid layer	0
Top solid layer	1

### 2.2. 3D Printing of the PDO Device and Sterilization Process

The PDO device was 3D printed according to the parameters in **Table 1**, and constructed as a flexible band with a perforated part connected to a locking case and a solid part (**Figure 1**). The 3D printed device was placed in Tyvek bags, sealed in a clean room and sterilized with ethylene oxide. Thereafter the bags were placed in aluminum foil pouches, dried under vacuum for at least seven days and then sealed in a moisture free environment.

### 2.3. In Vitro Degradation of the 3D Printed Device

In vitro degradation of the 3D printed PDO device was carried out under static conditions at 37 °C in phosphate buffered saline (PBS; pH = 7.4) from Sigma-Aldrich. The 3D printed device was cut into two segments in the middle of the perforated and solid parts to test the different bands separately. Thereafter, the perforated and solid bands were placed in a glass vial with septa containing 15 mL of PBS and retained in an oven at 37 °C for different aging times. After the aging times of 10, 28, and 140 days, respectively, the remaining devices and liquid phases were collected for further analysis. The remaining devices were placed in a conditioning room for mechanical testing. The devices were named with script of aging time according to PDO10, PDO28, PDO140, where the numbering corresponds to aging days. The neat PDO, before aging, was named PDO0. 3–4 devices were used for each aging time. After mechanical testing, the remaining devices were dried and kept under vacuum at room temperature

until characterization by other techniques. The remaining mass (%) of the 3D printed device after different aging times was calculated after dried under vacuum at room temperature according to Equation (1).  $m_t$  is the dry mass of the remaining device at aging time  $t$  and  $m_0$  is the initial mass of the device.

$$\text{Remaining mass} = \frac{m_t}{m_0} \times 100 \quad (1)$$

A pH-meter equipped with an Ag/AgCl electrode was used for measuring the pH of the liquid phases after aging. The electrode was calibrated with buffers solutions at pH 4 and 7.

#### 2.4. In Vivo Degradation of the 3D Printed Device

Degradation of the 3D printed PDO device was evaluated after aging subcutaneously in horses. Six horses and two ponies of mixed age, breed, and sex belonging to the SLU teaching herd were used. The aging times of 10 and 28 days were evaluated for the in vivo degradation and named similar to in vitro aged devices. The study was approved by the Uppsala Animal Ethics Committee, Dnr 5.8.18-18803/2018. In alignment with concurrent research on anesthetic recovery, the procedure was done under general anesthesia in the six horses. They were anesthetized according to a standard protocol<sup>[27]</sup> and placed in lateral recumbency on a medical foam mattress. The ponies were sedated as routine,<sup>[28]</sup> and local infiltration anesthesia with mepivacaine (Carbocaine) from Aspen Nordic was administered in an inverted L-block, at least 10 cm from the skin incision.

The surgical area was aseptically prepared. Via a skin incision, the PDO-device was inserted around a piece of fascia subcutaneously on the left or right side of the cranial trunk in a random order. By introducing the end of the band through the locking case, a self-locking loop was created. The loop was tightened and band protruding from the locking case was cut off, leaving 5 cm of the perforated part in the animal. A second PDO-device was inserted in the same manner on the opposite diagonal in the caudal aspect of the trunk. The skin was closed with USP 2-0 nonabsorbable suture (Prolene). For ethical reasons the animals were treated with meloxicam 0.6 mg kg<sup>-1</sup> per os (Metacam) from Boeringer Ingelheim Animal Health, on the day of surgery and for three consecutive days. The 3D printed devices were excised from the animals after 10 and 28 days, respectively. The procedure was performed under general anesthesia or sedation and local infiltration anesthesia according to the protocol described above. The band was immediately put in sterile plastic PP tubes for protection during transport. Within 2–6 h the band was dipped in liquid chromatography mass-spectrometry water from Merck to remove any remaining tissue and slightly dried on a paper. The devices were named according the same principal as the in vitro devices and placed in a conditioning room for mechanical testing. They were kept under vacuum at room temperature in between analysis.

#### 2.5. Characterizations of the 3D Printed PDO Device

The water-soluble degradation products after aging in vitro were analyzed with matrix assisted laser desorption/ionization-mass

spectrometry (MALDI-MS). Utilized instrument was a Bruker UltraFlex time-of-flight mass spectrometer with a SCOUT-MTP ion source equipped with a 337 nm nitrogen laser. The analyses were done in reflector mode with a filter for positive ions at an acceleration voltage of 25 kV and reflector voltage of 26.5 kV. Before the measurements, the liquid phase was mixed with 2-(4-hydroxyphenylazo)benzoic acid (HABA; 1 mg mL<sup>-1</sup>) from Supelco and sodium chloride (NaCl; 1 mg mL<sup>-1</sup>) in tetrahydrofuran from Merck at equal volumes, and drop-casted (0.5 μL) on the MALDI plate.<sup>[29]</sup> Furthermore, the low molar mass compounds present on remaining 3D printed devices after aging in vitro were compared. The devices were placed in chloroform (CHCl<sub>3</sub>) from Fischer Scientific for 24 h at room temperature and the extracted low molar mass compounds were mixed with HABA and NaCl, similar to the process for analysis of the products in the liquid phase. The compounds extracted from the devices after in vivo and in vitro aging of 28 days were further evaluated.

Fourier transform infrared spectroscopy (FTIR) absorption analysis of the perforated bands aged under in vivo and in vitro conditions was conducted at a resolution of 4 cm<sup>-1</sup> utilizing PerkinElmer Spectrum 100 instrument equipped with an attenuated total reflectance crystal accessory. All spectra were total area normalized. The tensile testing of the devices was performed on an Instron 5944 machine equipped with pneumatic grips and a 500 N load cell. The solid and perforated bands after in vitro, and bands after in vivo degradation conditions were placed in the conditioning room (23 ± 1 °C and 50 ± 5% relative humidity) for 40 h before the testing was performed. The measurements were run at speed of 10% min<sup>-1</sup> with a gauge length of 0.5 cm. The Young's modulus was calculated between the elongation of 2–5%. For each aging time, a replicate of 3–11 bands were evaluated. Relative molar mass of the devices was determined by size exclusion chromatography (SEC) and conducted on the GPCMAX instrument from Malvern with an autosampler at a flow rate of 0.5 mL min<sup>-1</sup>. The solvent was CHCl<sub>3</sub> with 2% v/v toluene from Fischer Scientific as an internal standard. Prior to the measurements, the perforated and solid bands from in vitro, and bands from in vivo aging, were dissolved in CHCl<sub>3</sub> (with 2% v/v toluene) at 40–45 °C and filtered with a Teflon filter (0.45 μm). The instrument was equipped with two PLGEL 5 μm MIXED-D columns. Calibration of the instrument was performed with narrow polystyrene standards ( $M_w = 1\ 200\text{--}400\ 000\ \text{g mol}^{-1}$ ). For each band or aging time, 2–3 bands were evaluated.

Thermal properties of the bands were measured by utilizing Mettler Toledo differential scanning calorimetry (DSC) 820 module. The perforated and solid bands aged in vitro, and bands aged in vivo were placed in an aluminum cup with a pinhole on the lid. Analysis was carried out through heating/cooling during three cycles from –30 to 200 °C at a rate of 10 °C min<sup>-1</sup> under a N<sub>2</sub> flow rate of 50 mL min<sup>-1</sup>. For each aging time, 3–7 bands were evaluated in the DSC runs. The scanning electron microscopy (SEM) images were acquired by Ultra high-resolution FE-SEM (Hitachi S4800) at an operating voltage of 2 kV. Prior to analysis, the perforated bands from in vitro conditions, and the bands from in vivo conditions, were placed on the SEM stub covered with a carbon tape. The samples were coated with Pt/Pd at a thickness of 3 nm. Wide angle X-ray diffraction (WAXD) analysis of the perforated and solid bands after in vitro aging, and bands after in vivo aging, was performed on a PANalytical

X'Pert PRO diffractometer equipped with a silica monocrystal sample holder. Cu  $\kappa$  alpha ( $\lambda = 1.541874$  nm) was operating at a voltage of 45 kV and a current of 40 mA. The intensity was measured at 2Theta ( $2\theta$ ) angular range between  $4^\circ$  and  $60^\circ$ .

### 3. Results and Discussion

A resorbable PDO device was manufactured by 3D printing to aid ligation of vascular tissue during surgical procedures in horses. The degradation and mechanical performance of the device were evaluated after different in vitro and in vivo aging times. In vitro aging enabled the analysis of remaining mass of the devices, pH changes and the analysis of formed water-soluble degradation products. In vivo aging was performed to assess the clinical suitability of the 3D printed PDO device and to identify any differences compared with the degradation process in vitro. The degradation profile and structural properties of the devices were monitored to understand the degradation induced and mechanical performance changes of the device, to ensure the performance in the intended application. Furthermore, the influence on the degradation of two different macroscopic structures of the device was evaluated.

#### 3.1. Degradation Profile

The 3D printed resorbable PDO device was constructed as a flexible band with two different macroscopic morphologies; a perforated part connected to a locking case and a solid part. A resorbable polymer device should retain adequate mechanical properties as surgical aid for the time required for the vascular tissue to reorganize, and finally degrade into water-soluble products in the body. The degradation product profile of the in vitro aged 3D printed device was therefore studied by MALDI-MS (Figure 2).<sup>[30]</sup> The analysis showed content of cyclic PDO ( $[\text{O}-\text{CH}_2-\text{CH}_2-\text{O}-\text{CH}_2-\text{C}=\text{O}]_n$ ) and linear PDO terminated with alcohol and acid end-groups ( $\text{H}-[\text{O}-\text{CH}_2-\text{CH}_2-\text{O}-\text{CH}_2-\text{C}=\text{O}]_n-\text{OH}$ ) after aging in simulated body conditions in PBS buffer at  $37^\circ\text{C}$  (Figure 3). In accordance, previous hydrolytic degradation studies of PDO suggested formation of linear acidic degradation products, e.g., hydroxyacids as a result of the hydrolysis of the ester bond of PDO.<sup>[31,32]</sup> The detected water-soluble oligomers were revealed after all evaluated aging times of 10, 28, and 140 days. Most of the products were cationized by  $\text{Na}^+$  and/or  $\text{K}^+$ , which are common adducts detected in MALDI-MS analysis after the addition of salt.

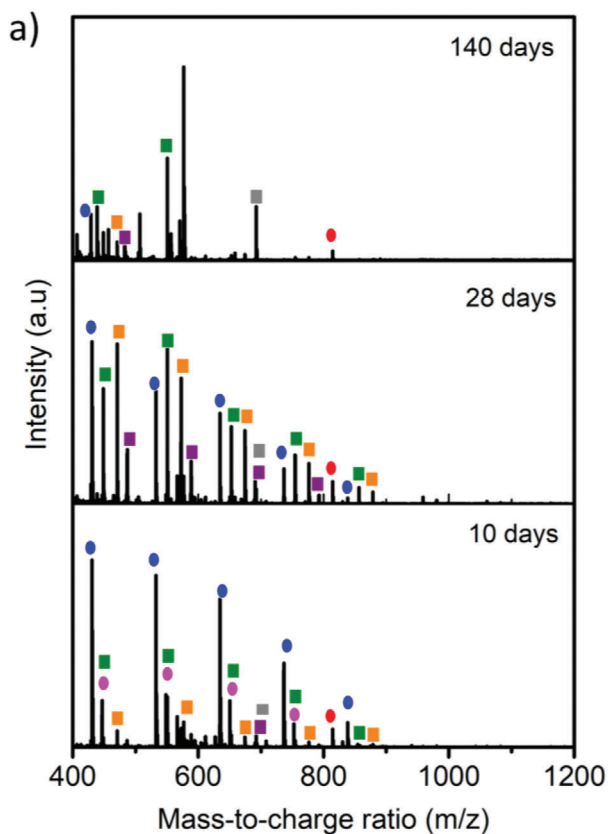
Two main trends were noticed for an aging time up to 28 days. First, the relative content of high molar mass water-soluble degradation products increased with aging time. This can be due to increased chain mobility and the larger space in the polymer matrix as consequences of degradation, which allowed for the release of the longer chains.<sup>[30]</sup> Second, the content of linear hydroxyacids increased over cyclic degradation products, which indicated that the hydrolysis of the cyclic products proceeded with aging time, either in liquid phase of the already released products, or through continued degradation of the device. The formation of acid degradation products can further catalyze the hydrolysis of the ester bonds and accelerate the degradation. After the longest aging time of 140 days, the relative amount of larger water-soluble

oligomers was lower in comparison to shorter oligomers. Furthermore, a smaller number of different products was detected in the PBS phase in comparison to the products detected in the samples with shorter aging times. This supports the further hydrolysis of the initially released hydroxyacids and cyclic oligomers.

To get a full picture of the degradation profile of the 3D printed devices, the low molar mass compounds remaining on the solid device were also analyzed by MALDI-MS (Figure 4; and Figure S1, Supporting Information). The remaining parts of the PDO devices were soaked in chloroform ( $\text{CHCl}_3$ ) after different aging times and the extracted degradation products were analyzed. Similar degradation products were attached to the 3D-printed devices as encountered in the PBS phase. Although, the relative number of degradation products with higher molar masses were greater in the extracted  $\text{CHCl}_3$  phase compared with the PBS phase (Figure S1, Supporting Information). This is probably due to the lower water solubility as well as migration rate of the higher molar mass compounds. Moreover, two additional series of linear PDO oligomers ( $\text{H}-[\text{O}-\text{CH}_2-\text{CH}_2-\text{O}-\text{CH}_2-\text{C}=\text{O}]_n-\text{O}-\text{CH}_2-\text{CH}_2-\text{OH} + \text{Na}^+$ ) and ( $\text{H}-\text{C}=\text{O}-\text{C}=\text{O}-[\text{O}-\text{CH}_2-\text{CH}_2-\text{O}-\text{CH}_2-\text{C}=\text{O}]_n-\text{OH} + \text{K}^+$ ) were detected at  $m/z$  1003, 1105, and 1031, 1133, respectively, after 10 and 28 days (Figure 3). These compounds were neither present on PDO140 nor PDO0. In the former case, probably due to the continued degradation with aging time and in the latter because of lower flexibility and compactness of the device before degradation, which lowered the migration rate. These two series of PDO oligomers might have been formed by thermal oxidation during the processing of the device as polyether-esters has been shown to be perceptible to thermo-oxidative degradation.<sup>[33]</sup>

It was further shown that the low molar mass products remaining on the devices after in vivo conditions were in good agreement with the ones present after in vitro aging with 28 days of aging time. One difference was the higher relative number of linear oligomers over cyclic oligomers after aging in vivo between  $m/z$  of 900–1200. Furthermore, additional functionalities to that of PDO were detected on the in vivo aged devices by FTIR as assigned to the wavenumbers 3250, 1650, and  $1530\text{ cm}^{-1}$  (Figure S2, Supporting Information). These additional functional groups were not detected on the in vitro aged devices. It is plausible that the functionalities were attributed to adsorbed proteins on the surface of the devices from the early stage of implantation,<sup>[34]</sup> where the peaks represented  $\nu\text{N}-\text{H}$ , Amide I ( $\nu\text{C}=\text{O}$ ,  $\nu\text{C}-\text{N}$ ) and Amide II ( $\delta\text{N}-\text{H}$ ,  $\nu\text{C}-\text{N}$ ), respectively. When the device was excised, a mild local inflammation was seen in the tissue around the implant. Macrophages and foreign-body giant cells can release degradative enzymes, reactive oxygen species and acid bioactive agents that can affect the degradation of biomaterials.<sup>[34]</sup>

As the MALDI-MS analysis showed content of degradation products including acid degradation products, the mass loss of PDO devices and pH of PBS solutions were further monitored (Figure 5). The remaining mass of the 3D printed device was still 99% after 10 days in vitro. Low initial mass loss has earlier been attributed to random chain scission during degradation of the amorphous parts,<sup>[31]</sup> which initially leads to formation of water-insoluble high molar mass products. The hydrolytic degradation of PDO likely begins with hydrolysis of amorphous parts that are more accessible to water and at later stages the crystalline parts of the polymer will be hydrolyzed.<sup>[32]</sup> The mass loss increased after



**b) Suggested assignments**

Cyclic	●	$[(\text{O}-\text{CH}_2-\text{CH}_2-\text{O}-\text{CH}_2-\text{C}=\text{O})_n]^+$	815
	●	$[(\text{O}-\text{CH}_2-\text{CH}_2-\text{O}-\text{CH}_2-\text{C}=\text{O})_n + \text{Na}]^+$	431, 533, 635, 737, 839, 941, 1043, 1145
	●	$[(\text{O}-\text{CH}_2-\text{CH}_2-\text{O}-\text{CH}_2-\text{C}=\text{O})_n + \text{K}]^+$	447, 549, 651, 753
Linear	■	$(\text{H}-[\text{O}-\text{CH}_2-\text{CH}_2-\text{O}-\text{CH}_2-\text{C}=\text{O}]_n-\text{OH} + \text{Na})^+$	449, 551, 653, 755, 857, 959, 1061, 1163
	■	$(\text{H}-[\text{O}-\text{CH}_2-\text{CH}_2-\text{O}-\text{CH}_2-\text{C}=\text{O}]_n-\text{OH} - \text{H} + 2\text{Na})^+$	471, 573, 675, 777, 879, 981, 1083, 1185
	■	$(\text{H}-[\text{O}-\text{CH}_2-\text{CH}_2-\text{O}-\text{CH}_2-\text{C}=\text{O}]_n-\text{OH} - \text{H} + \text{Na} + \text{K})^+$	487, 589, 691, 793, 895
	■	$(\text{H}-[\text{O}-\text{CH}_2-\text{CH}_2-\text{O}-\text{CH}_2-\text{C}=\text{O}]_n-\text{OH} + \text{H} + \text{Na} + \text{K})^+$	693
	■		

**Figure 2.** a) MALDI-MS of water-soluble degradation products in the PBS phase after aging in vitro for the different times in the  $m/z$  ranges 400–1200, b) the suggested identification of the detected water-soluble oligomeric adducts with corresponding  $m/z$  values.

28 days with a remaining mass of 94% due to continued hydrolysis further catalyzed by the more acidic medium.<sup>[31]</sup> Other studies observed that the mass loss of PDO sutures in buffer was minor up to at least 4–8 weeks, where after it increased gradually.<sup>[31,32]</sup> After 140 days of degradation, the remaining mass of the PDO device was only 33%, which led to shrinkage of the device upon

drying. It has been shown that the shrinkage of a PDO suture correlated with the mass loss during degradation.<sup>[35]</sup>

The pH of the PBS decreased from 7.4 after 10 days of degradation to 3.3 after 28 days. Thus, the capacity of the buffer was exceeded. The PBS was not regenerated during aging to be able to collect the released low molar mass degradation products. The

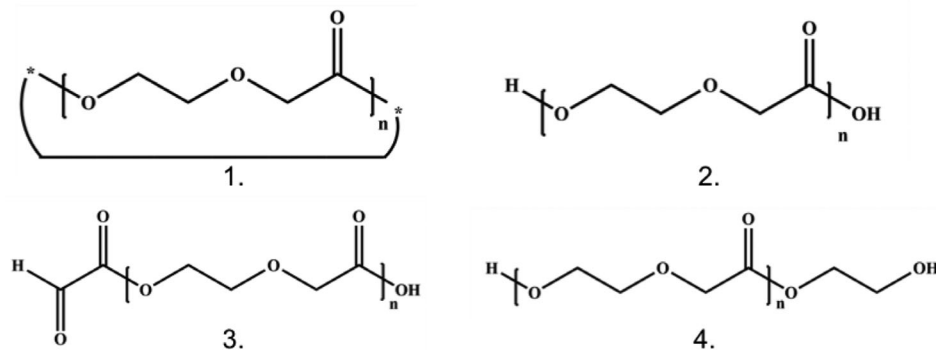


**Figure 3.** Suggested molecular structures for the series of oligomers detected in the PBS phase and remaining in the devices after aging in vitro and in vivo. 1. Cyclic oligomers, 2. Linear acid and hydroxyl terminated oligomers, 3. Aldehyde and acid terminated oligomers and 4. Oligomers terminated with two alcohol groups.

low pH indicated the formation of acid products and supported the MALDI-MS analysis. Other studies have shown that pH was relatively stable under longer aging times of PDO in comparison to this study.<sup>[31,32]</sup> The pH change during degradation of PDO may depend on several factors. The hydrolysis rate will be influ-

enced by the degree of crystallinity as amorphous parts of a polymer typically undergo faster degradation. Other influences are the outer conditions applied, such as temperature, medium, and the ratio between amount of device and medium. Furthermore, the contact area between device and the medium also plays an important role in the rate of degradation.<sup>[36]</sup> The processing of PDO will both influence the crystallinity and the macroscopic morphology, which determines the immediate contact with the medium. After the longest aging time of 140 days, the pH in the liquid phase had further decreased to 2.3.

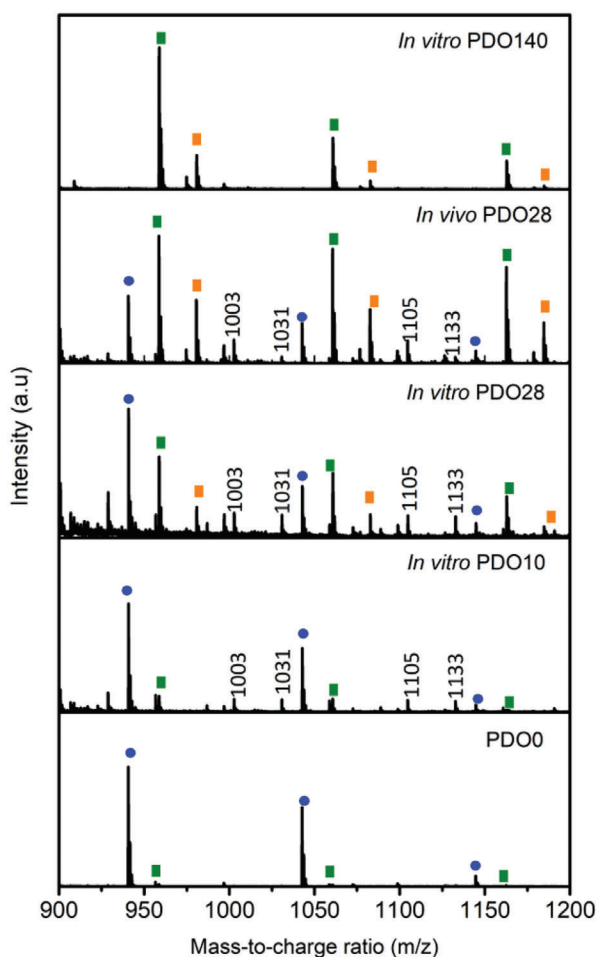


**Figure 4.** MALDI-MS of low molar mass products extracted from the devices subjected to in vitro conditions for different aging times, and in vivo for the aging time 28 days between m/z ratio 900–1200.

### 3.2. Mechanical Performance

It is essential to confirm the mechanical performance of the 3D printed resorbable devices after aging, as decreasing mechanical strength may jeopardize the intended support needed during tissue reorganization. Tensile testing was performed on the devices that had been subjected to in vivo and in vitro aging for the different time periods (**Figure 6** and **Table 2**). The mechanical performance of the remaining PDO devices was in general similar or inferior to the original PDO0 depending on the aging conditions and time. Overall, the PDO devices aged in vitro maintained their mechanical properties better compared with the devices aged in vivo during the same period. For in vitro devices, the Young's modulus ( $E$ ) and tensile strength at break ( $\sigma_b$ ) were relatively unchanged up to an aging of 10 days. However, the standard deviations increased with aging time as a result of small variations in the degradation process. It has previously been shown that changes in  $E$  and  $\sigma_b$  of PDO sutures were minor for aging in vitro especially during initial weeks of degradation.<sup>[8,9,37,38]</sup> It was depicted that the minor change in modulus of PDO after degradation was related to the low mass loss.<sup>[31]</sup> In the current study the decrement of strain at break ( $\epsilon_b$ ) was as large as 88% for perforated band after 10 days of aging. Similarly, it was reported that a PDO suture showed significant loss of strain after 14 days in PBS with pH 7.4 at 37 °C,<sup>[8]</sup> whereas the other mechanical properties were more resistant. Another degradation study of a PDO suture in similar conditions, but performed in Ringer's solution, showed that the strain was relatively constant after aging for 56 days.<sup>[37]</sup>

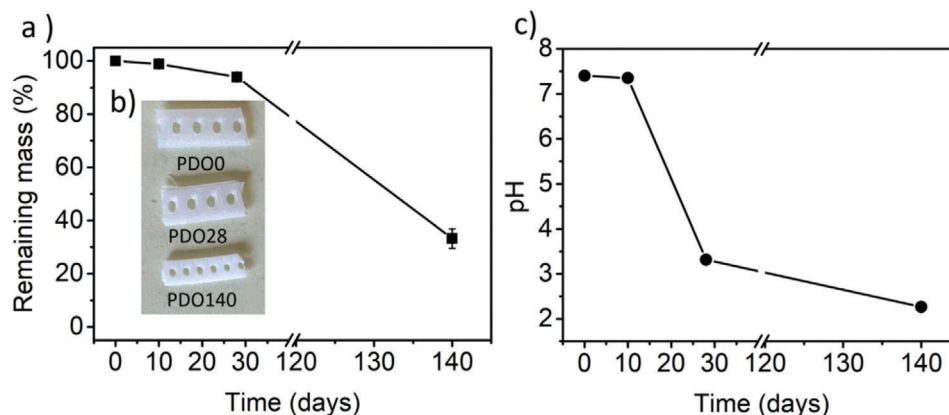


**Figure 5.** Remaining mass of the 3D printed devices a), an image showing part of the perforated band of PDO0, PDO28, and PDO140 b) and the changes of pH in liquid phase (PBS) after aging times of 0, 10, 28, and 140 days c).

The modulus and strength of the device were seriously agitated after in vitro aging for 28 days. The perforated band could not be tested due to fragility, whereas the solid band had a strength reduction of 84% compared with the original solid PDO0 band. Similarly, PDO stents and sutures subjected to PBS at 37 °C displayed a significant reduction in mechanical properties after 28 days of degradation.<sup>[8,39]</sup> After the initial rapid decrease, the strain at break remained relatively constant during further aging. The perforated band showed initially slightly higher modulus and strength values compared with the solid band. Whereas, the strain at break values of the perforated bands were similar to those of the solid bands at all aging times. Resembling results were encountered after in vitro degradation of a comparable device made through injection molding of poly(glycolide-*co*-trimethylene carbonate) triblock copolymer.<sup>[30]</sup>

The in vivo aging resulted in completely different impact on the mechanical behavior of the devices compared with the devices aged in vitro. It was not possible to test mechanical properties of the remaining in vivo devices after 28 days due to fragmentation of the band into small parts. The corresponding  $E$  and  $\sigma_b$  values for in vivo aged devices decreased by 28% and 54% after only 10 days, respectively. The strain at break after aging in vivo showed a loss of strain at break of up to 95%, which was matching the values of in vitro aging. Previously, in vivo incubation of a PDO suture in rabbit fascia and peritoneal cavity showed significant loss of breaking strength after 28 days, whereas the strength of the suture was retained in Ringer's lactate.<sup>[40]</sup> A PDS suture placed subcutaneously in rats for 42 days further demonstrated a significant strength reduction.<sup>[41]</sup> Enhanced in vivo degradation was suggested to be due to the presence of phagocytes and their release of reactive oxygen species in case of a poly(trimethylene carbonate-*co*-*D,L*-lactic acid) copolymer.<sup>[42]</sup> On the other hand, another study demonstrated that the in vitro degradation had slightly more negative effect on the mechanical strength of PDO sutures compared with aging under in vivo conditions, which was explained by the more severe and static conditions.<sup>[7]</sup> In addition to variations of polymer structure and characteristics and exact aging conditions, the differences in manufacturing, i.e., 3D-printing and anatomic location of the device within the animal might influence the aging process.

The initial degradation of the polymer during aging was most likely connected to scission of the tie chains in the amorphous parts,<sup>[31,35]</sup> whereas the following loss in mechanical properties may be related to the decreasing molar mass caused by hydrolysis of ester bonds. As expected, the relative molar mass decreased steadily with aging time in vitro and in vivo (Figure 7; and Table S1, Supporting Information). The devices, thus, degraded significantly even though the mass losses were relatively low during the same time period. This is typical for the hydrolysis process, which initially is characterized by decreasing molar mass and limited mass loss. It correlates with the random chain scission of the amorphous parts in the beginning of the degradation process.<sup>[31]</sup> During the second stage, accelerated mass loss rate is typically observed due to formation of water-soluble degradation products.<sup>[43]</sup> The largest reduction in molar mass was observed between 10 and 28 days of aging. As an example, the mass average molar mass ( $M_w$ ) decreased from 52 000 for PDO10 to 20 200 g mol<sup>-1</sup> for PDO28 perforated bands after in vitro aging. This correlated with the mass loss and pH drop that was evident after 28 days in comparison to the shorter aging times.

The molar masses of the devices were similar after aging in vivo and in vitro conditions for almost all aging times. An exception was PDO28 that had slightly greater molar mass after aging in vivo compared with aging in vitro conditions. The dispersity ( $\mathcal{D}$ ) of the PDO devices after in vitro and in vivo aging could further reveal differences in degradation profiles (Table S1, Supporting Information). The  $\mathcal{D}$  of in vitro aged devices was constant at 1.9 up to 10 days for the perforated band, after which it decreased to 1.6 after 28 days. It is anticipated that the differences in lengths of the polymer chains increase in the beginning of degradation and decrease with longer aging times due to the release of water-soluble products from the devices.<sup>[42]</sup> Whereas, the  $\mathcal{D}$  during aging in vivo was constantly 2.0 and independent of aging time. It was shown that a larger dispersity of PDO stem from enhanced surface degradation compared to bulk degradation.<sup>[44]</sup> Furthermore, the relative molar masses of the perforated and solid bands after in vitro were similar for all aging times considering the large standard deviations. A longer degradation time could have led to larger differences in the molar masses of perforated and solid

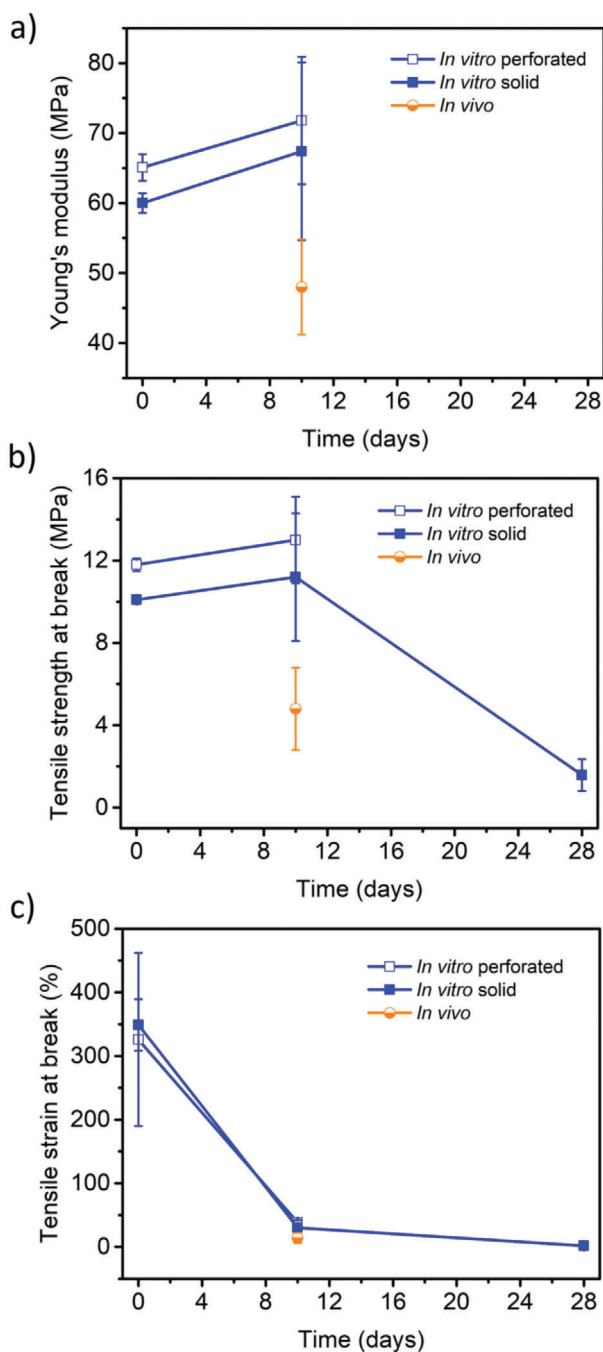


**Figure 6.** Young's modulus a), tensile strength at break b) and tensile strain at break c) of 3D printed PDO devices after different aging times.

bands. The molar mass of PDO140 could, however, not be evaluated due to insolubility in  $\text{CHCl}_3$ .

DSC evaluation gave further insights into the degradation process and the observed changes in the mechanical performance of the PDO devices. As references, the specific enthalpy of fusion ( $\Delta H_{m1}$ ) of PDO0 before aging was  $72 \text{ J g}^{-1}$  and that of PDSII suture was  $85 \text{ J g}^{-1}$ . This demonstrated the influence of material processing on crystallinity since the heat of fusion is pro-

**Table 2.** Mechanical properties of the 3D printed devices subjected to *in vitro* and *in vivo* aging.

Parameters <sup>a)</sup>			$E$ [MPa]	$\sigma_b$ [MPa]	$\epsilon_b$ [%]
PDO0	-	Perforated	$65.1 \pm 1.9$	$11.8 \pm 0.3$	$325.8 \pm 140$
		Solid	$60.0 \pm 1.4$	$10.1 \pm 0.2$	$348.9 \pm 40$
PDO10	<i>In vitro</i>	Perforated	$71.8 \pm 9.1$	$13.0 \pm 2.1$	$38.3 \pm 3.8$
		Solid	$67.4 \pm 13$	$11.2 \pm 3.1$	$30.2 \pm 2.5$
	<i>In vivo</i>		$48.0 \pm 6.8$	$4.8 \pm 2.0$	$14.2 \pm 8.3$
PDO28	<i>In vitro</i>	Perforated	-	-	-
		Solid	-	$1.58 \pm 0.8$	$1.81 \pm 0.7$
	<i>In vivo</i>		-	-	-

<sup>a)</sup>  $E$ —Young's Modulus,  $\sigma_b$ —Tensile strength at break,  $\epsilon_b$ —Elongation at break.

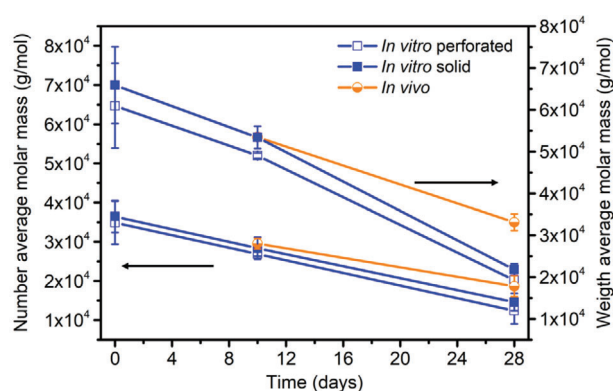


**Figure 7.** Number average and mass average molar masses obtained through SEC for 3D printed PDO devices after *in vitro* and *in vivo* aging.

portional to the crystallinity of the polymer. The  $\Delta H_{m1}$  of the 3D printed PDO devices during first heating cycle was constant up to 10 days and increased after 28 days for devices aged both *in vivo* and *in vitro* (Figure 8; and Table S2, Supporting Information). The observed insolubility of *in vitro* PDO140 in  $\text{CHCl}_3$  may be due to high crystallinity, which had further increased after 28 days. Several studies have shown that the crystallinity of PDO increases with aging time.<sup>[8,32]</sup> The increment of crystallinity with aging time is expected to occur as the amorphous parts of a polymer degrade before the crystalline parts. In addition, it has been suggested that the greater movement of shorter chains and heating above the glass transition of PDO (below room temperature before degradation) can enable the rearrangement of the loose chains into crystals.<sup>[35]</sup> In the present study, the change in melting temperature was minor up to 28 days. After that, the melting temperature of the *in vitro* perforated PDO140 band decreased to  $93 \text{ }^\circ\text{C}$  from the initial  $110 \text{ }^\circ\text{C}$  for PDO0. This decrease is probably a result of the decreased molar mass and could also indicate that the degradation of the crystalline parts of the device was proceeding.<sup>[32]</sup>

The *in vivo* aged devices displayed slightly lower specific enthalpy of fusion and higher melting temperature compared with *in vitro* aged devices after 28 days. Whereas, there was no difference in the glass transition temperature ( $T_g$ ) of *in vivo* and *in vitro* aged devices during second heating cycle. The  $T_g$  could decrease as a consequence of decreasing molar mass.<sup>[32]</sup>

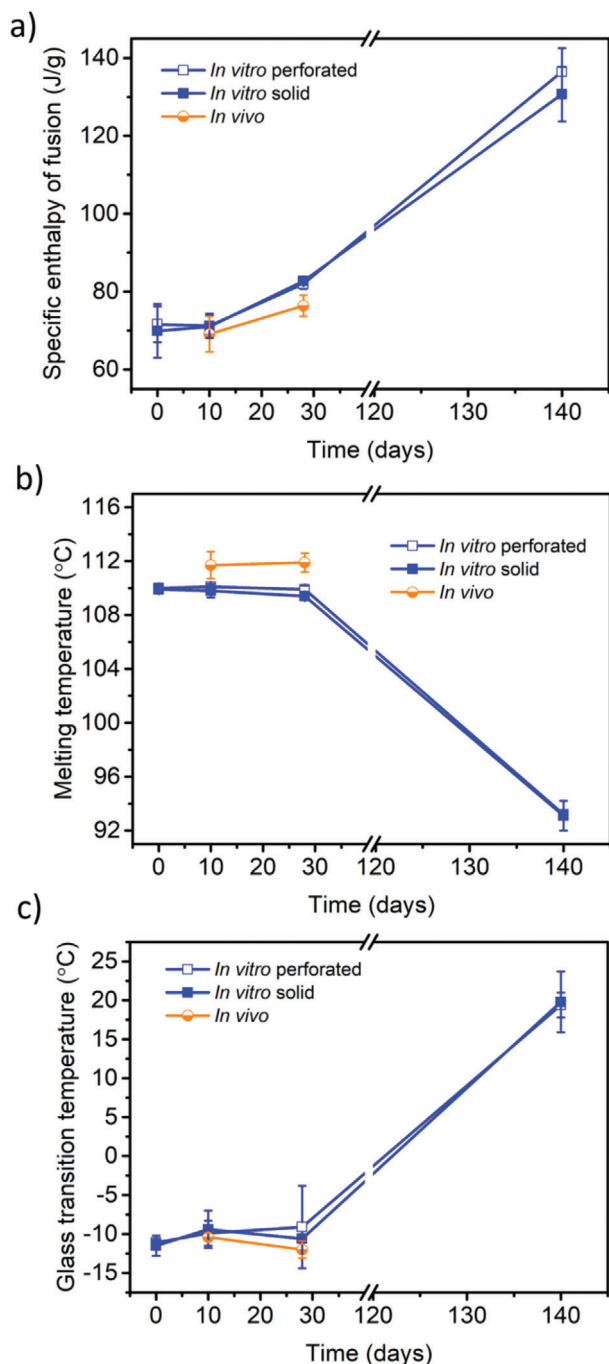


**Figure 8.** The specific enthalpy of fusion a), melting temperature b) and glass transition temperature c) of 3D printed PDO devices after different aging times.

The absence of changes may be due to increased crystallinity with aging time, which restricts the movement of chains and could counteract the effect of decreasing molar mass. After 140 days, the  $T_g$  of PDO had increased to 20 °C from  $\approx -10$  °C for the shorter aging times. Here, the crystallization during cooling probably gave rise to more imperfect or thinner crystals as indicated by the lower melting temperature, which also lowered

the flexibility of the material. There were minor differences in the thermal properties of perforated and solid bands.

### 3.3. Morphological Changes

The SEM analysis provided additional understanding of the degradation process and mechanical performance of the 3D printed PDO devices after in vivo and in vitro aging (Figure 9). Furthermore, the analysis gave insights into the degradation of the different macroscopic morphologies of the device after in vitro conditions. Both PDO0, before degradation, and PDO10 after in vitro aging, displayed the appearance of spherical crystals at microscale that were partly connected to each other. Similar crystal morphology of PDO was previously observed after both melt crystallization<sup>[45]</sup> and solution casting.<sup>[46]</sup> After 28 days of aging in vitro, the separate crystals became more diffused and displayed a continuous phase of the polymer. A similar appearance of the surface of the device could be noticed already after 10 days of in vivo aging. Since the degradation rate in terms of crystallinity and molar mass was comparable between devices from in vitro and in vivo aging after 10 days, the variance in surface appearance most likely resulted from the different environments. During in vivo, the device was placed in nonstatic system with extracellular fluid composition acting to keep homeostasis while changing over time depending on the actual status of local inflammation. The device is also subjected to an immunologic defence system and dynamic movement from the muscles in the horses. In vitro, the device was placed in a closed system in PBS solution under static condition.

After 140 days in vitro and 28 days in vivo aging the PDO matrix became apparently ruptured. The in vivo PDO140 was not tested since the device fragmented into small pieces already after 28 days. As viewed in the SEM images, especially of the in vivo PDO28 device, areas of apparent degradation were illustrated by holes in the polymer matrix. The holes are likely due to degradation of amorphous parts, but the presence of macrophages and their release of reactive oxygen species could have enhanced the degradation.<sup>[47]</sup> A histological evaluation of in vivo device after 10 days showed adhesion of macrophages to the device, which sustained that degradation of PDO during in vivo aging led to loss of small pieces.<sup>[48]</sup> Furthermore, phagocytosis have earlier been observed of various types and sizes of plastics.<sup>[49]</sup> It was first after the longest aging time in vitro, 140 days, that the appearance of cracks in the PDO matrices were noticed for both perforated and solid bands. Similarly, it was previously shown that surface cracks and detachment of surface layers of PDO suture appeared after 120 and 150 days in PBS at 37 °C, respectively.<sup>[8]</sup> As previously outlined, the degradation depends on several parameters, such as crystallinity, conditions, and morphology of PDO. For instance, PDO films, solution casted and thermally processed through extrusion and melt compounding displayed large cracks after only 42–59 days at similar conditions.<sup>[46,50]</sup>

The SEM images of the perforated and solid bands of PDO140 indicated that there was a difference in degradation process depending on the different morphologies of the device (Figure 9). In the perforated band, the appearance of larger spherical crystals was still prominent even though they were still closely positioned to each other after drying. The solid band, on the other hand,

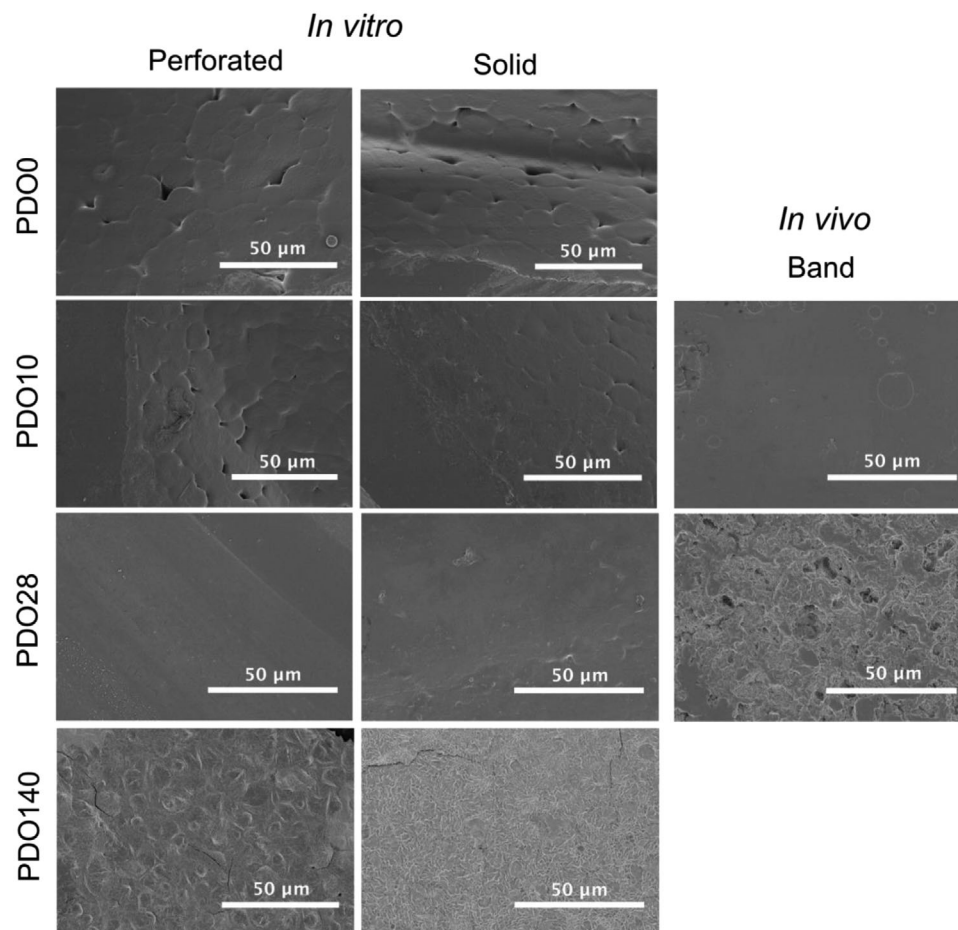


**Figure 9.** SEM images of devices after different aging times in vitro and in vivo.

showed appearance of narrowly located fibers within the polymer matrix. This indicated that there is a difference in the degradation process of the perforated and solid bands. As earlier outlined, the PDO28 solid band was still intact, whereas the perforated band was too fragile to be mechanically analyzed. It has been stated that the processing and following orientation of lamellae of PDO filaments influenced the location of degradation.<sup>[7,31,32,39,45]</sup> The resulting cracks from degradation of amorphous parts of PDO were found to be oriented perpendicular to the fiber direction to the most part, which was suggested to be due to interlamellar degradation. Furthermore, it was shown that water medium gave rise to longitudinal cracks owing to the more efficient interfibrillar water swelling due to fewer tie chains compared with between the lamellar structures.<sup>[45]</sup>

The crystalline character of the 3D printed devices was further investigated by wide angle X-ray diffraction (WAXD) (**Figure 10**). All PDO devices, before and after aging, showed content of a crystalline phase. The devices acquired after the in vitro and in vivo conditions displayed two reflections by WAXD as earlier shown for PDO.<sup>[35,39]</sup> They were located at 22.2° and 23.7° for the in vitro perforated bands. There was no change in peak positions for any of the devices up to an aging time of 28 days. Hence, the degradation primarily occurred in the more amor-

phous parts of PDO. Similar was encountered after degradation of PDO sutures in PBS buffer at 37 °C for up to around 65 days.<sup>[35]</sup> It was concluded that the unit cells did not distort by the degradation. After 140 days, the reflection at 22.2° for the perforated band, and both reflections for the solid band, shifted to lower  $2\theta$ . It was assumed that this was a result of the hydrolytic degradation of some crystalline parts of the PDO device, and in line with the thermal analysis revealing lower melting temperature of PDO140 compared with devices acquired after shorter aging times and the original PDO0.

The perforated and solid bands, including PDO0, displayed different peak positions, which were preserved at all aging times. It was shown that the solid bands exhibited slightly lowered  $2\theta$  of the two peaks compared with the perforated bands. Thus, the two different macroscopic morphologies of the device displayed distortions, or different  $d$ -spacings, of the crystallites. We speculate that the temperature gradient during cooling of the device on the 3D printing bed was slightly different for the perforated and solid parts of the band. As well established, polylactide forms two crystalline structures when melt processed at different temperatures.<sup>[51]</sup> The difference in  $d$ -spacings of crystallites may in turn have influenced the degradation of the perforated and solid bands as seen by SEM and XRD, but needs more evaluation.

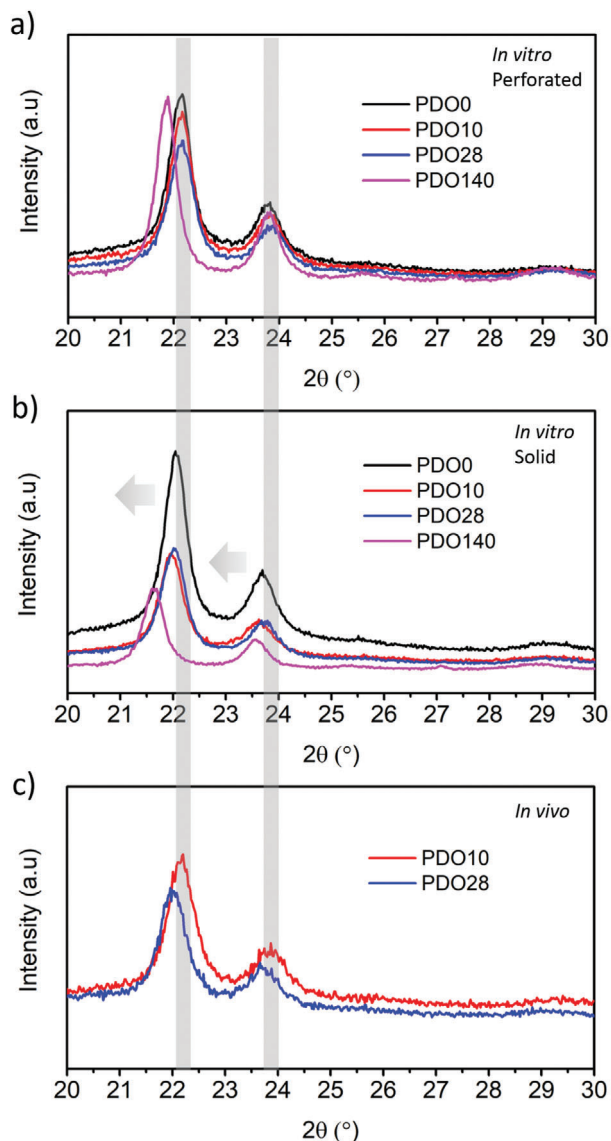


**Figure 10.** WAXD of 3D printed PDO devices of perforated part a), solid part of the band b) and after in vivo c) at different aging times.

## 4. Conclusions

A resorbable 3D printed PDO device for ligation of vascular tissues in horses was tested. The degradation profile and mechanical performance of the device were fingerprinted and compared during aging in vivo and in vitro. During aging, both cyclic and linear degradation products of PDO were released into the PBS solution, where the relative number of linear counterparts increased with time. Analysis of the low molar mass compounds remaining in the devices, revealed that the in vivo device displayed content of additional linear degradation products in comparison with the in vitro aged device. After 10 days of aging, the Young's modulus and strength at break of the in vivo aged devices had decreased by 28% and 54%, respectively. However, the corresponding values of in vitro aged devices were still similar to the PDO device before degradation. After 28 days, the aging gave

rise to significant deterioration of mechanical performance and the in vivo aged devices had fragmented into small parts exhibiting clear holes in the PDO matrix. Any apparent visible cracks of the in vitro aged device were first significant after 140 days. Furthermore, two parts of the device with different macroscopic morphologies displayed divergence in degradation as seen by appearance and crystallite peak positions after 140 days. This shows the importance of in vivo testing of bioresorbable devices and further highlights the influence of different morphologies on the degradation of resorbable polymer devices.

## Supporting Information

Supporting Information is available from the Wiley Online Library or from the author.

## Acknowledgements

K.H.A. and I.S. contributed equally to this work. The authors thank Sweden's Innovation Agency, Vinnova, for financial support (Grant No. 2018-04278).

## Conflict of Interest

Author O.V.H. is the inventor of the self-locking device and founder of company Resorbable Devices AB. The company holds the associated patents; the inventor did not perform the laboratory analysis. The other authors declare that they have no known competing financial interests or personal relationships that could have appeared to influence the work reported in this paper.

## Data Availability Statement

Research data are not shared.

## Keywords

3D printing, biomedical materials, degradation products, polydioxanone, resorbable device

Received: April 19, 2021  
Revised: June 14, 2021  
Published online: August 2, 2021

- [1] C. K. S. Pillai, C. P. Sharma, *J. Biomater. Appl.* **2010**, *25*, 291.
- [2] D. K. Gilding, A. M. Reed, *Polymer* **1979**, *20*, 1459.
- [3] K. Rajbabu, N. J. Barber, W. Choi, G. H. Muir, *Ann. R. Coll. Surg. Engl.* **2007**, *89*, 359.
- [4] J. A. Martins, A. A. Lach, H. L. Morris, A. J. Carr, P.-A. Mouthuy, *J. Biomater. Appl.* **2020**, *34*, 902.
- [5] M. Mohseni, D. Huttmacher, N. Castro, *Polymers* **2018**, *10*, 40.
- [6] J. A. Ray, N. Doddi, D. Regula, J. A. Williams, A. Melveger, *Surg., Gynecol. Obstet.* **1981**, *153*, 497.
- [7] J.-T. Hong, N.-S. Cho, H.-S. Yoon, T.-H. Kim, M.-S. Koh, W.-G. Kim, *J. Appl. Polym. Sci.* **2006**, *102*, 737.
- [8] H. L. Lin, C. C. Chu, D. Grubb, *J. Biomed. Mater. Res.* **1993**, *27*, 153.

- [9] C. M. Kearney, C. T. Buckley, F. Jenner, P. Moissonnier, P. A. J. Brama, *Equine Vet. J.* **2014**, *46*, 494.
- [10] J. N. Im, J. K. Kim, H.-K. Kim, C. H. In, K. Y. Lee, W. H. Park, *Polym. Degrad. Stab.* **2007**, *92*, 667.
- [11] G. Molea, F. Schonauer, G. Bifulco, D. D'angelo, *Br. J. Plast. Surg.* **2000**, *53*, 137.
- [12] S. M. Cokelaere, A. M. J. G. Martens, P. Wiemer, *Vet. Surg.* **2005**, *34*, 651.
- [13] M. P. De Bont, *Equine Vet. Educ.* **2018**, *30*, 255.
- [14] R. H. Carpenter, *J. Am. Anim. Hosp. Assoc.* **1972**, 718.
- [15] C. S. Ferreira, A. Ferreira da Silva Caldas, A. P. Martinez de Abreu, F. Sartori, A. Maciel Crespilho, A. P. Ferreira, G. Mendes Gomes, K. da Cunha Peixoto, Jr., A. Maciel Crespilho, *Andrology* **2015**, *4*, 1000149.
- [16] R. E. Werner, A. J. Straughan, D. Vezin, *J. Am. Vet. Med. Assoc.* **1992**, *200*, 64.
- [17] A. S. Macedo, Í. Dos Santos Dal-Bó, A. Mendes de Quadros, G. Brambatti, K. D. H. Lemos dos Reis, M. Veloso Brun, M. Meller Alievi, C. Afonso de Castro Beck5, *Acta Sci. Vet.* **2012**, *40*, 1.
- [18] C. R. Almeida, T. Serra, M. I. Oliveira, J. A. Planell, M. A. Barbosa, M. Navarro, *Acta Biomater.* **2014**, *10*, 613.
- [19] O. V. Höglund, R. Hagman, K. Olsson, J. Mindemark, N. Borg, A.-S. Lagerstedt, *Acta Vet. Scand.* **2011**, *53*, 47.
- [20] O. V. Höglund, J. Ingman, F. Södersten, K. Hansson, N. Borg, A.-S. Lagerstedt, *BMC Res. Notes.* **2014**, *7*, 825.
- [21] K. Ishigaki, O. V. Höglund, K. Asano, *Vet. Surg.* **2021**, <https://doi.org/10.1111/vsu.13623>.
- [22] M. Guvendiren, J. Molde, R. M. D. Soares, J. Kohn, *ACS Biomater. Sci. Eng.* **2016**, *2*, 1679.
- [23] A. Ahlinder, S. Charlton, T. Fuoco, J. Soulestin, A. Finne-Wistrand, *Polym. Degrad. Stab.* **2020**, *181*, 109372.
- [24] S. Dänmark, A. Finne-Wistrand, K. Schander, M. Hakkarainen, K. Arvidson, K. Mustafa, A. C. Albertsson, *Acta Biomater.* **2011**, *7*, 2035.
- [25] J.-H. Shim, J.-Y. Won, J.-H. Park, J.-H. Bae, G. Ahn, C.-H. Kim, D.-H. Lim, D.-W. Cho, W.-S. Yun, E.-B. Bae, C.-M. Jeong, J.-B. Huh, *Int. J. Mol. Sci.* **2017**, *18*, 899.
- [26] L. Dong, S.-J. Wang, X.-R. Zhao, Y.-F. Zhu, J.-K. Yu, *Sci. Rep.* **2017**, *7*, 13412.
- [27] M. Wiklund, I. Granswed, G. Nyman, *Vet. Anaesth. Analg.* **2017**, *44*, 1139.
- [28] G. Nyman, S. Marntell, A. Edner, P. Funkquist, K. Morgan, G. Hedenstierna, *Acta Vet. Scand.* **2009**, *51*, 22.
- [29] G. Adamus, M. Hakkarainen, A. Höglund, M. Kowalczyk, A.-C. Albertsson, *Biomacromolecules* **2009**, *10*, 1540.
- [30] N. Aminlashgari, O. V. Höglund, N. Borg, M. Hakkarainen, *Acta Biomater.* **2013**, *9*, 6898.
- [31] M. A. Sabino, S. González, L. Márquez, J. L. Feijoo, *Polym. Degrad. Stab.* **2000**, *69*, 209.
- [32] M. A. Sabino, J. Albuerne, A. J. Müller, J. Brisson, R. E. Prud'homme, *Biomacromolecules* **2004**, *5*, 358.
- [33] G. Botelho, A. Queirós, P. Gijsman, *Polym. Degrad. Stab.* **2000**, *68*, 35.
- [34] J. M. Anderson, A. Rodriguez, D. T. Chang, *Semin. Immunol.* **2008**, *20*, 86.
- [35] C. Ping Ooi, R. E. Cameron, *J. Biomed. Mater. Res.* **2002**, *63*, 280.
- [36] L. Wu, J. Ding, *J. Biomed. Mater. Res. A.* **2005**, *75A*, 767.
- [37] D. A. Müller, J. G. Snedeker, D. C. Meyer, *J. Orthop. Surg. Res.* **2016**, *11*, 111.
- [38] K. M. Tobias, C. E. Kidd, P.-Y. Mulon, X. Zhu, *Vet. Surg.* **2020**, *49*, 550.
- [39] C.-M. Han, E. Lih, S.-K. Choi, T. M. Bedair, Y.-J. Lee, W. Park, D. K. Han, J. S. Son, Y. K. Joung, *J. Ind. Eng. Chem.* **2018**, *67*, 396.
- [40] S. A. Metz, N. Chegini, B. J. Masterson, *Biomaterials* **1990**, *11*, 41.
- [41] D. Greenwald, S. Shumway, P. Albear, L. Gottlieb, *J. Surg. Res.* **1994**, *56*, 372.
- [42] Z. Ma, Y. Wu, J. Wang, C. Liu, *Regen. Biomater.* **2017**, *4*, 207.
- [43] M. Hakkarainen, A.-C. Albertsson, S. Karlsson, *Polym. Degrad. Stab.* **1996**, *52*, 283.
- [44] J. Cai, K. J. Zhu, S. L. Yang, *Polymer* **1998**, *39*, 4409.
- [45] Y. Márquez, L. Franco, P. Turon, J. Martínez, J. Puiggalí, *Polymers* **2016**, *8*, 351.
- [46] A. P. T. Pezzin, E. A. R. Duek, *Polym. Degrad. Stab.* **2002**, *78*, 405.
- [47] K.-H. Lee, C. C. Chu, *J. Biomed. Mater. Res.* **2000**, *49*, 25.
- [48] I. Sjöberg, O. V. Höglund, O. Wattle, in *ACVS Surgey Summit 2020, Virtual Sessions*, Wiley, Veterinary Surgery, **2020**, pp. 1–98.
- [49] V. J. Tomazic-Jezic, K. Merritt, T. H. Umbreit, *J. Biomed. Mater. Res.* **2001**, *55*, 523.
- [50] S.-C. Chen, X.-L. Wang, Y.-Z. Wang, K.-K. Yang, Z.-X. Zhou, G. Wu, *J. Biomed. Mater. Res. A.* **2007**, *80A*, 453.
- [51] J. Zhang, Y. Duan, H. Sato, H. Tsuji, I. Noda, S. Yan, Y. Ozaki, *Macromolecules* **2005**, *38*, 8012.